Quantitative evaluation of emission properties and thermal hysteresis in the mid-infrared for a single thin film of vanadium dioxide on a silicon substrate

Gianmario Cesarini [*,1,2], Grigore Leahu[1], Alessandro Belardini[1], Marco Centini [1], Roberto Li Voti[1], Concita Sibilia[1]

[1]Dipartimento di Scienze di Base ed Applicate per l'Ingegneria, Sapienza Università Roma
Via A. Scarpa 16, 00161 Rome, Italy
[2]I.N.F.N. Sezione di Roma, Piazzale Aldo Moro 2, 00185 Rome, Italy

* Corresponding author: tel. +39 06 4976 6594 Fax +39 06 4424 0183
e-mail: gianmario.cesarini@uniroma1.it

Abstract

We present a comparative study of the emission properties of a vanadium dioxide thin film (approximately 200 nm) deposited on a silicon wafer in different sub-spectral-ranges of the mid-infrared, with particular attention to the windows of transparency of the atmosphere to the infrared radiation (i.e., 3-5 μm, 8-12 μm). The infrared emission properties of the structure are closely related to the well-known phase transition of the first order, from semiconductor to metal, of the vanadium dioxide around the temperature of 68 °C. The characterization of the emissivity in the sub-regions of the mid-infrared was carried out both in the front configuration, that is on the VO_2 film side, and in the rear configuration on the silicon wafer side, and showed a strong difference in the hysteresis thermal bandwidth, in particular between the short wave region and the long wave region. The bandwidth is equal to 12°C for the front and 15°C for the rear. The emissivity behaviors as a function of temperature during the semiconductor-metal transition in the mid-infrared subregions were analyzed and explained using the theories of the effective medium of Maxwell Garnett and Bruggeman, highlighting the greater functionality of one theory or the other depending on the spectral detection band.

Keywords: Phase change materials; Thermochromism; Infrared radiometry; Tunable emissivity.

1. Introduction

There is considerable interest in emissivity engineering for applications ranging from infrared emitters to heat management and thermal labeling/imaging [1-7]. In determining emissivity for various materials and structures, Kirchhoff's law of thermal radiation is commonly used and states that the emissivity of an object is equal to its wavelength-dependent absorptivity. An approach to emissivity engineering has been to select materials with an adequate dispersion law to obtain a selective thermal emission, while a complementary approach involves the superficial structure, both disordered and ordered as for the photonic crystals. In addition, optical antennas and metamaterials have also been employed to tailor the directionality and the spectrum of thermal emission [8,9]. For the purpose of emissivity engineering the use of transition metal oxides is proving to be very functional due to their promising electrical and optical properties, and in particular thermochromic materials can play a significant role in various fields of applications [10-14]. These materials have temperature-dependent optical properties that can be used to modulate the emissivity, and a significant advantage of modulation based on thermochromic materials is that it allows "passive smart devices" that can operate without the need for external control or supply power. An attractive thermochromic material is vanadium dioxide (VO_2) [15,16], a related oxide in which a thermally induced transition

from semiconductor to metal (SMT) occurs near room temperature (T_C ~ 68 °C in bulk crystals), which carries the material from an insulating state to a metallic one. This material for its switching properties is interesting in various fields of application, from optical telecommunication modulators [17,18], to passive aerospace radiators [19,20], to military infrared camouflage [21-23], up to the memristors for electronic memories [24,25].

The core of this work is to show the spectral dependence as a function of the detection band of the emission properties in the mid-infrared sub-regions of a structure consisting of a vanadium dioxide film deposited on a silicon substrate. This goal has been achieved through an accurate method of temperature-dependent radiometric measurements and a detailed analysis using the theories of the effective medium, in particular Maxwell Garnett and Bruggeman. In this paper we would like to investigate which is the most appropriate model to follow the semiconductor to metal transition of emissivity, that is fundamental to design and realize a new class of optimized infrared devices operating during the phase transition, where the coexistence of the monoclinic and rutile states takes place. For this purpose we are interested to investigate the mechanism of the emissivity switch in the different detection bands, which could be differently sensitive to the clusters formation process inside the vanadium dioxide film.

2. Material and methods

2.1 Sample description

The tested sample consists of a VO_2 thin film with a thickness of about 200 nm deposited on a 480 µm mirror-polished silicon wafer; the VO_2 layer has been deposited by means of reactive radio frequency sputtering with a substrate temperature of 500 °C. The average roughness of the film σ = 20 nm has been determined using the atomic force microscope (Fig. 1).

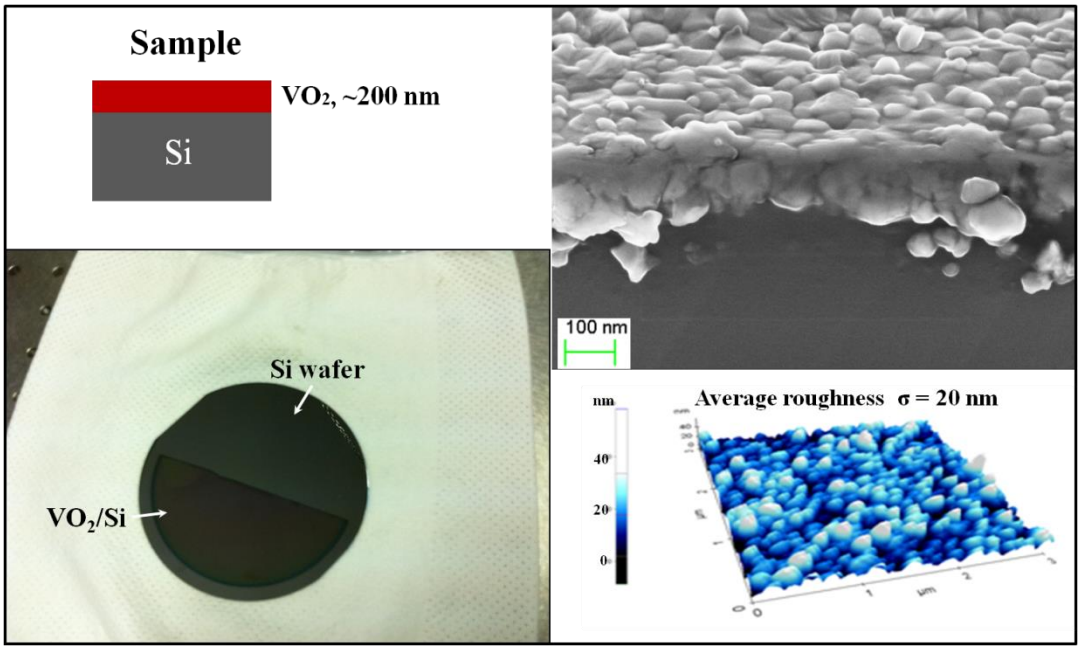

Fig. 1 On the left side the sample scheme (above) and the sample image (below); on the right side the SEM image (above) and the 3D profilometry reconstruction through the AFM (below).

2.2 Experimental setup

In order to characterize the variations of the optical and emission properties with the temperature and as a consequence of the semiconductor-metal transition of the vanadium dioxide, has been chosen the silicon substrate because it is

transparent to the infrared radiation at the wavelengths of interest for this study. The emissivity has been calculated indirectly by the Kirchhoff's law of thermal radiation from the reflection and transmission measurements as a function of the temperature, and only the reflection measurements were performed both in the front configuration and in the rear configuration, the transmission being obviously the same for both configurations. Kirchhoff's law states that for an arbitrary body at a fixed temperature that emits and absorbs thermal radiation in the thermodynamics equilibrium, the emissivity is equal to the absorptivity, and therefore:

$$\varepsilon(\lambda) = \alpha(\lambda) = 1 - \rho(\lambda) - \tau(\lambda), \qquad (1)$$

where $\varepsilon(\lambda)$ is the spectral emissivity, and $\alpha(\lambda)$, $\rho(\lambda)$, $\tau(\lambda)$ are the spectral absorptivity, reflectivity and transmissivity, respectively. This is a classic and very efficient method, but not the only one that allows to obtain the emissivity by following the phase transition [26]. Recently C. L. Gomez-Heredia *et al.* have obtained excellent results for this purpose through the thermal-wave resonant cavity technique [27]. In order to perform the temperature scanning measurements in the 30°C-100°C range the sample has been posed in contact with an electrical heater. A globar lamp has been used as a source of infrared radiation and kept at a temperature of about 130 °C through a stabilized power supply. The radiation was modulated at 36 Hz by a mechanical chopper (ORTEC 9479) before reaching the sample under test, and the same frequency is used for the external reference of the lock-in amplifier (Perkin-Elmer 7265) that provides data acquisition. The reflectance measurements have been performed at near-normal incidence, and in order to perform the transmittance measurements at normal incidence as a function of sample temperature, a central hole of 10 mm in diameter has been realized in the copper body of the electrical heater, used for the sample temperature scan. The infrared radiation, both in the setup for reflection and transmission measurements, has been detected by a (HgCdZn)Te photovoltaic IR detector. In order to observe the differences induced by the vanadium dioxide transition (SMT) as a function of the detection band, two different detectors were used: the first with 2.5 – 5 μm detection band, for the characterization of emission properties in the SWIR region (Vigo System model PVI-2TE-5, quadrant cells 2 x 2 mm^2), and the second with a detection band of 2 – 12 μm for the MIR region (Vigo System model PVI-4TE-10.6, quadrant cells 1 x 1 mm^2). The characterization in the LWIR region was performed by coupling to the latter detector a long pass filter with transmission of 90 % in the 8 – 12 μm range and complete suppression of shorter wavelength. The current temperature of the sample is measured by a copper-constantan thermocouple, and, in view of the low sample heat capacity, has been used a type with thin and coated wires of 0.5 mm diameter (type TG-40-T, NY Thermoelectric Co., Inc.), in addition to a thermal flat with high thermal conductivity (RS Pro 554-311), consisting of metal oxide powders, to minimize the thermal resistance at the point of contact with the sample; and therefore the temperature measurement is performed by means of a digital multimeter (HP 34401A). The temperature scan of the sample is performed in a quasi stationary regime, realized by changing linearly the sample temperature slowly with time, with a speed of about 1 °C/min. A germanium lens has been placed at the distance 2f (f = 50 mm is the focal length) from both the sample surface and the detector so that the image of the investigated zone of the sample has been projected to the active area of the detector with an enlargement 1:1. In order to obtain the transmissivity, the transmittance measurements have been normalized with respect to the reference signal without sample, while those of reflectance compared to the reference signal from a flat gold mirror (a gold thin film deposited on a silicon wafer of the same thickness as the sample). See Fig.2 for the scheme of the experimental setup.

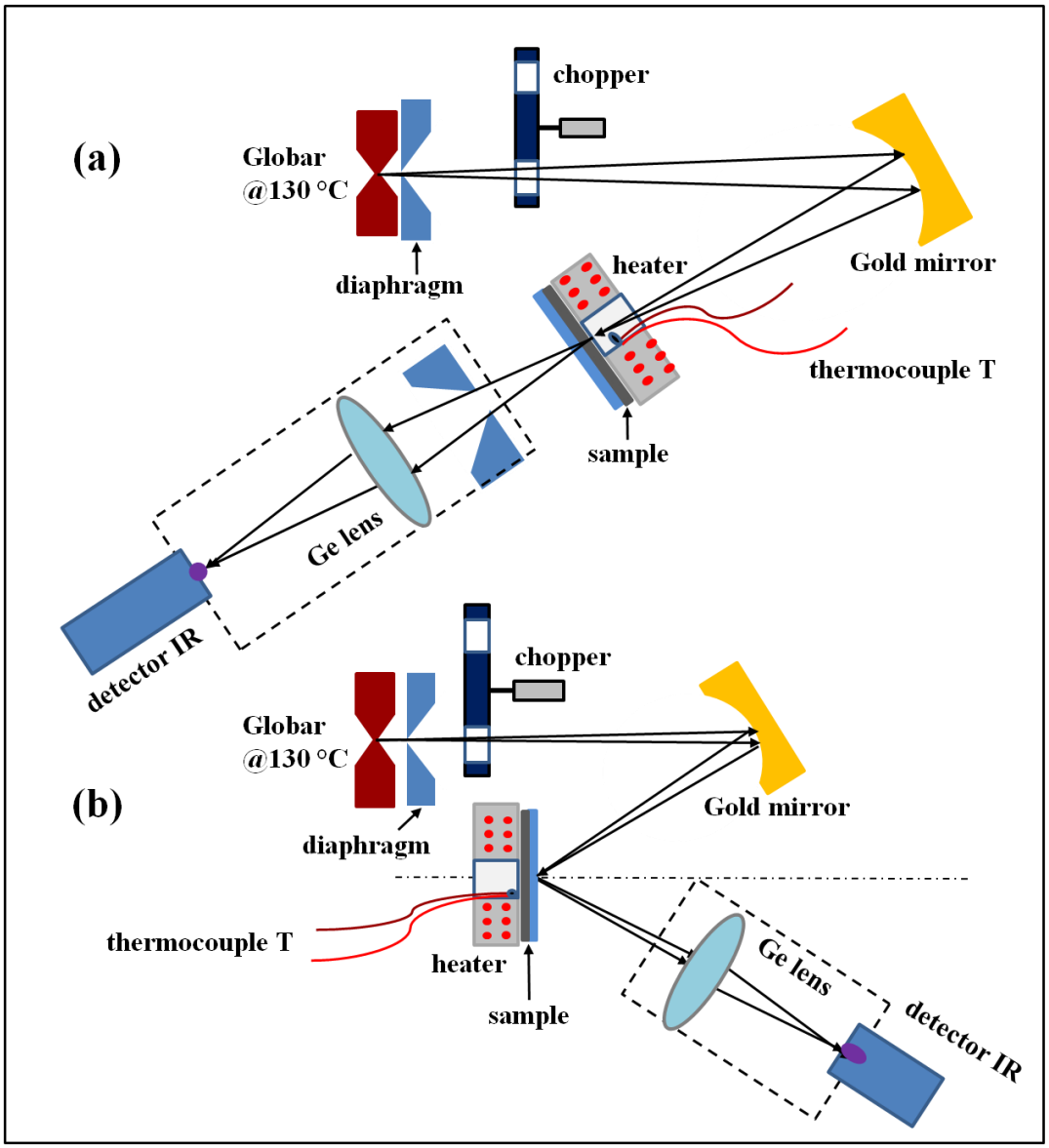

Fig. 2 Schematic analysis of experimental setup for transmittance (a) and reflectance (b) measurements, in the reflection setup the angle of incidence is wide for clarity.

3. Results and discussion

Transmittance and reflectance measurements as a function of temperature have been therefore performed using three spectral detection bands: SWIR (2.5 – 5 μm), MIR (2 – 12 μm) and LWIR (8 – 12 μm). The characteristics of the emission thermal hysteresis, derived from Kirchhoff's thermal radiation law (Eq. 1) and shown in Figs 3-4, indicate how the variations induced by the phase transition of VO_2, from the spectral point of view, occur mainly in the cooling cycle, against a substantially coincident heating cycle.

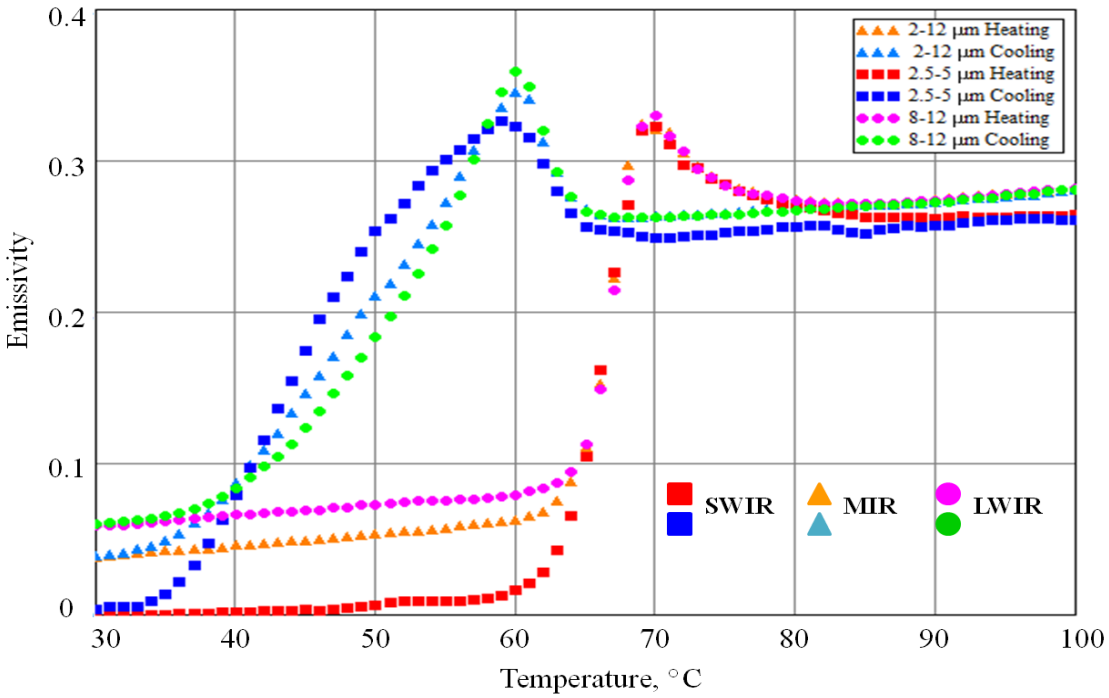

Fig. 3 SWIR, MIR and LWIR emissivity vs sample temperature for the VO_2/Si structure in the *front* configuration.

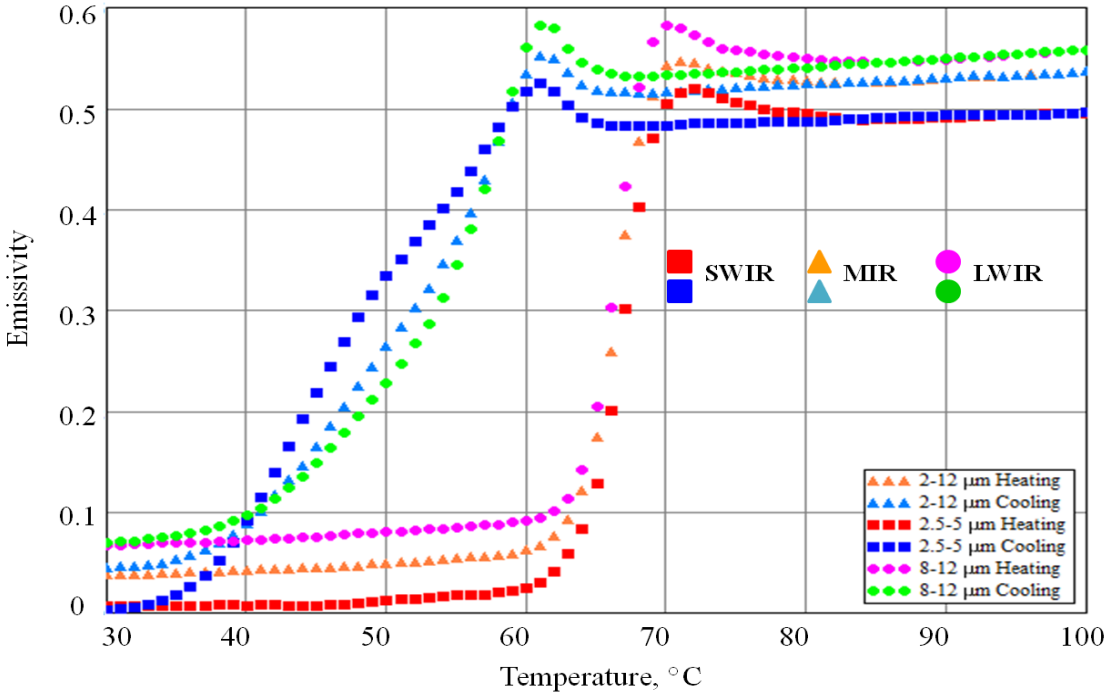

Fig. 4 SWIR, MIR and LWIR emissivity vs sample temperature for the VO_2/Si structure in the *rear* configuration.

In order to quantify the differences, in terms of emission properties, induced by the phase transition of VO_2 with the temperature by varying the spectral detection band, have been introduced three evaluation parameters:

- *transition temperature* T_C, given by the temperature corresponding to the maximum of the emissivity derivative with respect to the temperature $\left.\frac{\partial \varepsilon}{\partial T}\right|_{max}$ and thus indicating the maximum induced emissivity variation by semiconductor-metal transition (heating) or metal-semiconductor (cooling);

- *thermal bandwidth* ΔT_C, given by the difference $T_{CH} - T_{CC}$ between the T_C of the heating cycle (T_{CH}) and that of the cooling cycle (T_{CC});

- *differential emissivity* $\Delta\varepsilon_{HL}$, given by the difference $\varepsilon_H - \varepsilon_L$ between the high-temperature (ε_H @100°C) and low-temperature (ε_L @30°C) emissivity values respectively corresponding to the metal and semiconductor phase of vanadium dioxide.

From the experimental data, therefore, the values of the above parameters have been extrapolated for the evaluation of the emission properties of the considered structure in the three spectral bands SWIR, MIR and LWIR. The values are reported in Table 1.

Configuration	**Spectral band (μm)**	**T_C (°C)**		**ΔT_C (°C)**	**$\Delta\varepsilon_{HL}$**
		Heating	**Cooling**		
Front	**SWIR (2.5 – 5)**	66.5	43.5	22.5	0.26
	MIR (2 – 12)	66	55.5	11.5	0.24
	LWIR (8 – 12)	67	56.5	10.5	0.22
Rear	**SWIR (2.5 – 5)**	66.5	43.5	23	0.50
	MIR (2 – 12)	66	57.5	8.5	0.50
	LWIR (8 – 12)	66	58	8	0.49

Tab. 1 Extrapolated values for the front and rear configurations.

Starting from the observation of the transition temperatures in the Tab. 1 we see a substantial coincidence of the three temperatures, according to the definition above, in the sample heating cycle. On the other hand, considering the cooling cycle, the difference between the transition temperatures is considerably larger, in particular passing from the short-wave to the long-wave infrared region: between the SWIR and LWIR thermal bandwidths there is a difference of 12 °C in the case of the front configuration and of 15 °C in the case of the rear one. These values indicate that under the aspect of the radiative emission the phase transition of the vanadium dioxide induces a maximum speed of variation of the emissivity on a much wider temperature scale for the SWIR. The thermal bandwidth is a parameter closely related to the manufacturing process, and to some factors such as annealing temperature or growth temperature [28-31]. The differentials of emissivity passing from the configuration front to the rear one are subject to a notable increase being $\Delta\varepsilon_{HL}$ the double one for the SWIR ($\Delta\varepsilon_{HL}$ from 0.26 to 0.50) and greater than the double for the LWIR ($\Delta\varepsilon_{HL}$ from 0.22 to 0.49). Now considering the average emissivity value corresponding to the three transition temperature of the heating cycle we obtain $\varepsilon_f^* = 0.2$ for the front configuration and $\varepsilon_r^* = 0.3$ for the rear; at this point, observing at which temperatures the same emissivity value occurs for the SWIR and LWIR hysteresis (the thermal hysteresis for the MIR is

always intermediate to these two) we obtain both, for the front and for the rear configuration, a difference of ~5 °C. This last difference can be for example significant in thermal camouflage applications [32].

Furthermore, there is an anomalous and more significant emission [33] in the front configuration, for both cycles; this emissivity peak coincides for the heating cycle for all detection bands and its presence was also observed by means of the infrared passive thermography (CX320 COX Co., range 8 – 14 μm). This peak of emissivity is clearly shown in Fig. 5, where the temperatures below the thermograms are the real ones as measured by the thermocouple. It is worth noting that in this case the heater is a polished aluminum plate which is chosen to homogenize the operation temperature of the vanadium dioxide sample, without producing any effects in the sample emittance due to the low emissivity of aluminum (ε_{Al} = 0.05).

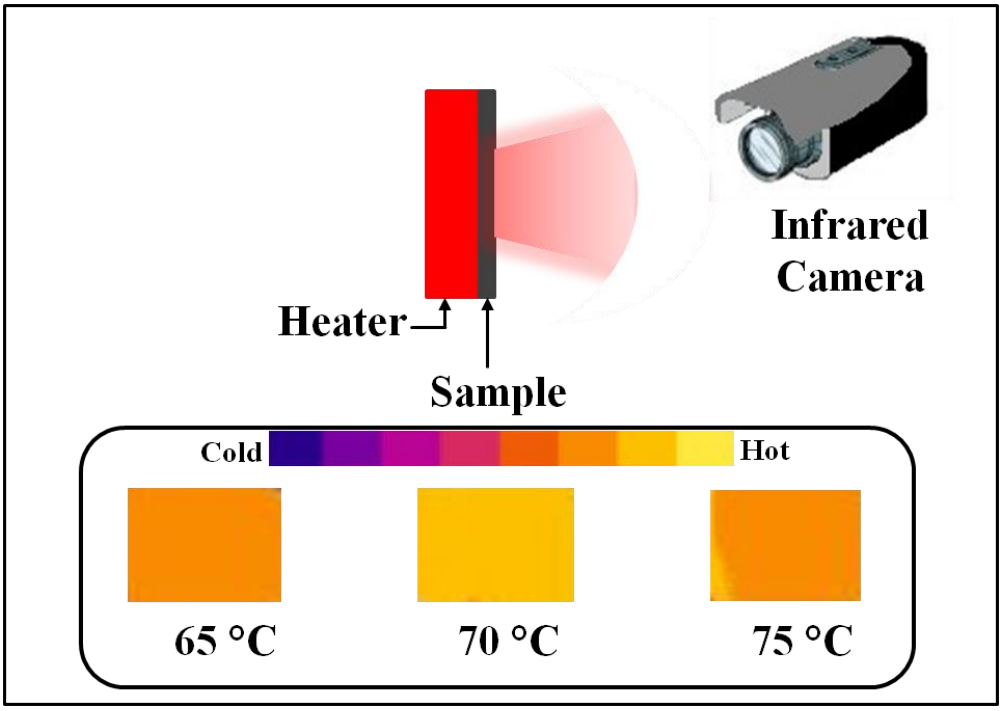

Fig. 5 The color bar indicates the apparent temperature while the temperatures below the images are the real ones (front configuration); the lighter and brighter color of the thermogram at 70 °C indicates a greater emissivity than the other two temperatures, thus highlighting the anomalous emission that occurs towards the end of the phase transition and linked to the coexistence of the semiconductor and metal phases.

4. Theoretical modeling

In order to explain the experimental results of the temperature-dependent emissivity in the SWIR, MIR and LWIR sub-regions, we used a theoretical approach for numerical simulations based on the following criteria: we have assumed that the Globar source is a black body at the temperature of 130 °C; in order to simplify the simulations, for the VO_2 film we have introduced effective optical constants n and k (refractive index and extinction coefficient, respectively) averaged in the SWIR, MIR and LWIR sub-regions; in order to analyze the semiconductor-metal transition (SMT) of the VO_2 film, during the heating and cooling cycles from 30 °C to 100 °C and vice versa, the theory of the effective medium was used, and in this case the theories of Maxwell Garnett and Bruggeman. The procedure for determining the effective optical constants n and k concerned all the spectral detection bands, SWIR, MIR and LWIR, and for the VO_2 it consisted in obtaining the refractive index n and the extinction coefficient k in the two semiconductor and metal states [34]. As regards the phase of coexistence of states and the evaluation of the transition through the theory of the effective

medium, this last study involved only SWIR and LWIR, coinciding with the windows of transparency of the atmosphere to the infrared radiation. The average values, relative to the three spectral detection bands in the semiconductor state and in the metallic state, of the refractive index and of the extinction coefficient were determined by the best fit between experimental results and numerical simulations; for the calculations are used the data supplied by Li (1980) for silicon between 1.2 μm and 14 μm at the temperatures of 293 K and 400 K. First of all, therefore, the average optical constants of vanadium dioxide far from the transition zone al temperatures of 30 °C (semiconductor state) and 100 °C (metallic state) have been calculated from the contemporary fit of the transmissivity T, and of the reflectivity in the front (R_f) and rear (R_r) configurations. The following table (Tab. 2) shows the optical constants obtained for the three spectral bands for the semiconductor and metallic VO_2.

Spectral band (μm)	**VO_2 (30 °C) $n_S + ik_S$**	**VO_2 (100 °C) $n_M + ik_M$**
SWIR (2.5 – 5)	$2.46 + i(1.78 \cdot 10^{-3})$	3.07 + i5.05
MIR (2 – 12)	2.49 + i0.07	4.69 + i6.1
LWIR (8 – 12)	2.51 + i0.19	5.74 + i6.05

Tab. 2 Extrapolated values for the average optical constants: refractive index and extinction coefficient, where the subscripts s and m indicate the semiconductor and metal states, respectively.

These values are in line with what is present in the literature considering the strong dependence on manufacturing processes. The error for fitting simultaneously T, R_f and R_r is on average 1%.

The study of the VO_2 phase transition continued with the use of the theories of the effective medium to be able to describe the trend of the emissivity as a function of the temperature during the heating and cooling cycles from 30 °C to 100 °C. According to a similar approach, during a quasi-static phase transition, in the semiconductor-metal composite the volumetric fraction of the metal phase is quantified by the filling factor *f*, while $1 - f$ is the residual volume fraction in the semiconductor phase. The resulting optical properties of the inhomogeneous compound were obtained by a weighted combination of the properties of the two phases according to well-established theories of Maxwell Garnett and Bruggeman [35-39]. In accordance with this criterion, the inclusions have been supposed of spherical shape and have been considered to be very small compared to the wavelength of the incident radiation. Let us now analyze the expressions of the permittivity of the effective means corresponding to the inhomogeneous semiconductor-metal composite of VO_2. The permittivity of the inhomogeneous composite is given by the following formula for the approach according to the theory of Maxwell Garnett:

$$\varepsilon(f) = \varepsilon_S \frac{\varepsilon_M(1+2f) + 2\varepsilon_S(1-f)}{\varepsilon_M(1-f) + \varepsilon_S(2+f)} \qquad (2)$$

where $\varepsilon_S = (n_S + ik_S)^2$ is the permittivity of VO_2 in the semiconductor state, while $\varepsilon_M = (n_M + ik_M)^2$ is the permittivity of VO_2 in the metallic state, and they have been calculated using the constants n and k shown in Tab. 3 for SWIR and LWIR. Regarding the approach according to the Bruggeman theory, the permittivity is given by the following formula:

$$\varepsilon(f) = \frac{[\varepsilon_M(f-q) + \varepsilon_S(1-f-q)] \pm \sqrt{[\varepsilon_M(f-q) + \varepsilon_S(1-f-q)]^2 + 4(1-q)q\varepsilon_M\varepsilon_S}}{2(1-q)} \qquad (3)$$

where, also in this case, where $\varepsilon_S = (n_S + ik_S)^2$ is the permittivity of VO_2 in the semiconductor state, and $\varepsilon_M = (n_M + ik_M)^2$ is the permittivity of VO_2 in the metallic state for SWIR and LWIR, while q is a geometric factor that in the case of the approximation of spherical inclusions is equal to q = 1/3 (the fit of the experimental data with the aforesaid model always considers the solution with a positive imaginary part). Therefore, the filling factor *f* remains the only parameter free to estimate in order to evaluate the emissivity variation induced by the vanadium dioxide phase transition. Below are shown (Figs 6 and 7) the fit of the emissivity trends as a function of the temperature in the front and rear configurations through the homogenization's models of the permittivity ε of Maxwell Garnett and Bruggeman for SWIR and LWIR.

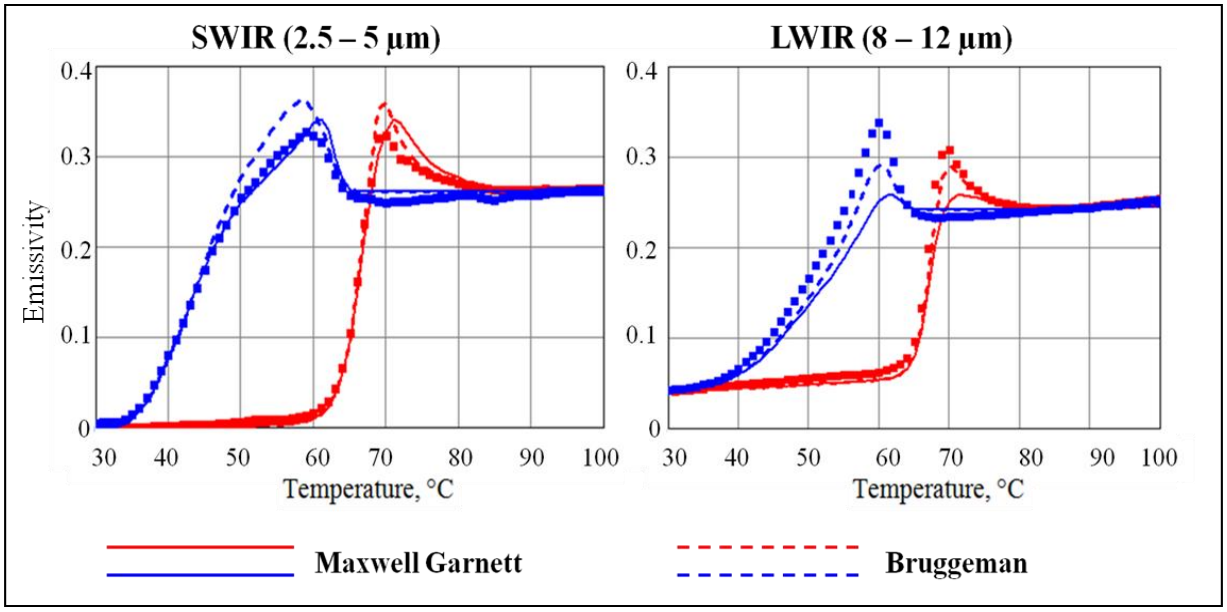

Fig. 6 Fit of the experimental trends of the emissivity as a function of the temperature in the ***front configuration*** for the spectral band SWIR (left) and for the LWIR (right) with the homogenization models of Maxwell Garnett and Bruggeman.

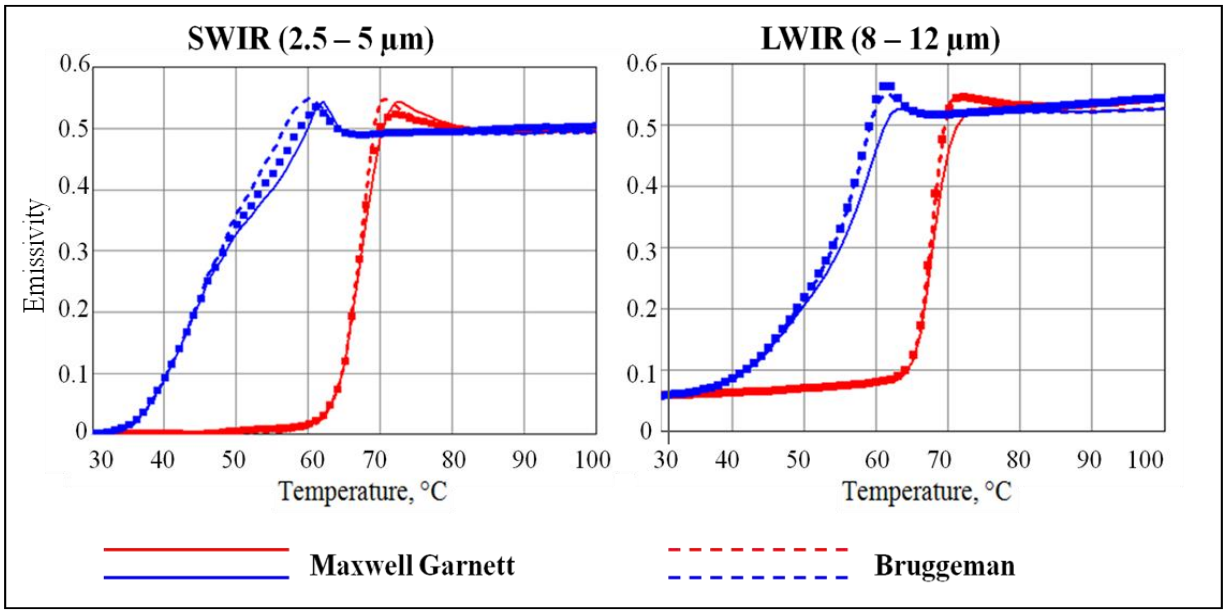

Fig. 7 Fit of the experimental trends of the emissivity as a function of the temperature in the ***rear configuration*** for the spectral band SWIR (left) and for the LWIR (right) with the homogenization models of Maxwell Garnett and Bruggeman.

As shown in the figures 6 and 7, the model that responds in the best way to the variation induced on the emissivity of the structure from the VO_2 phase transition is that of Maxwell Garnett for SWIR and that of Bruggeman for LWIR.

The MG model is able, in particular, to follow very well the metal-semiconductor transition in the cooling cycle for the front configuration and to replicate the emission peaks in the two cycles with levels close to the experimental ones, albeit slightly translated to higher temperatures. In the rear configuration we also find a very good agreement between the fit with the MG model and experimental data, and in particular in the identification of the peak in the cooling cycle.

For LWIR, the Bruggeman model provides a trend that is closer to that of the emissivity data as a function of temperature. In the rear configuration the adhesion with the experimental data is almost perfect, except for a slight discrepancy on the final high temperature emissivity level. In the front configuration the identification, with respect to the experimental data, of the temperatures at which the emission peaks are located is excellent (in this case 70 °C for the heating cycle and 60 °C for the cooling cycle), while the levels of emissivity of the peaks are lower [$\Delta\varepsilon_{exp,mod}$ = 0,05 (@ 60 °C); $\Delta\varepsilon_{exp,mod}$ = 0,02 (@ 70 °C)].

Finally, here is shown (Fig. 8) a comparison between the trends of the volumetric fractions *f* related to the Maxwell Garnett model for SWIR and to the Bruggeman model for LWIR.

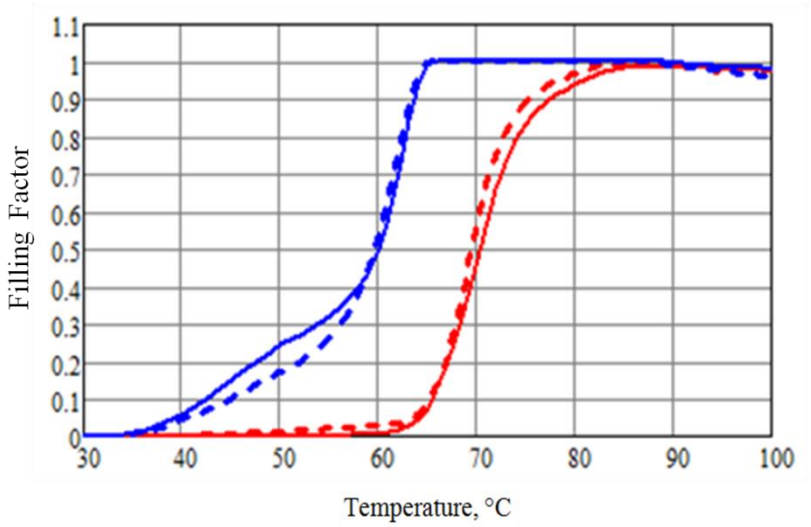

Fig. 8 The solid line represents the trend of the volumetric fraction *f* for the Maxwell Garnett model (SWIR); the dotted line for the Bruggeman model (LWIR).

The thermal hysteresis of the two volumetric fractions f_1 (MG, SWIR) and f_2 (B, LWIR) vary between an initial level equal to 0 (VO_2 semiconductor) and a final level equal to 1 (VO_2 metal), and it is to be noted that the hysteresis of f_2 is closer than that of f_1 by virtue of the greater sensitivity of the detection of SWIR to smaller domains.

It is interesting to observe the differences between the values of the volumetric fractions of the two models and corresponding to the emissivity peaks present in the heating and cooling cycles for the SWIR and LWIR front configurations:

f_1 (MG, SWIR)	0.58 (@61 °C)	0.55 (@71 °C)
f_2 (B, LWIR)	0.54 (@60 °C)	0.55 (@70 °C)

Tab. 3 Extrapolated values for the volumetric fractions relative to the emissivity peaks.

Also the values shown above in the Tab. 3 indicate how the structure of the vanadium dioxide film and silicon substrate responds differently depending on the detection spectral band, a 4% difference being present between the f_1 (MG, SWIR) and f_2 (B, LWIR) corresponding to the emission peaks present in the cooling cycle. Overall, the phenomenon of the anomalous emission for both the models and for both the spectral bands occurs for the values of the volumetric fraction *f* of the metallic phase in the range 0.3 – 0.7. These models can therefore be used to dimension even multilayer structures in order to optimize their performance in terms of emissivity by using the properties of the effective medium during the phase transition of the vanadium dioxide [40-43].

5. Conclusions

In conclusion, the emission properties of the structure of the vanadium dioxide film on silicon substrate show a difference in terms of thermal bandwidth ($\Delta T_{C,SL} = \Delta T_{C,SWIR} - \Delta T_{C,LWIR}$) equal to 12 °C for the front configuration and 15 °C for the rear configuration. This indicates how the dynamics of the phase transition under the aspect of the emission occur in two very different temperature ranges for the spectral bands SWIR and LWIR, compared to a transition temperature T_C substantially coinciding for the three bands in the heating cycle (see Tabs 1 and 2). For the emissivity differentials $\Delta\varepsilon_{HL}$, the rear configuration shows an emissivity variability dynamics about twice that of the front configuration, i.e. an average $\Delta\varepsilon_{HL,av} = 0.50$ for the three intervals in the rear case compared to a $\Delta\varepsilon_{HL,av} = 0.24$ in the front one. The results obtained through the theoretical modeling have shown that the theory of Maxwell Garnett is

the most suitable for the description of the transition in the case of SWIR, while that of Bruggeman the most suitable in the case of LWIR, thus revealing in the latter case a greater interaction between inclusions. This dependence of the emission properties with the spectral band for the different response of the film to longer or shorter wavelengths and with consequent different modeling is linked to the larger or smaller size of the clusters, and to the phenomenon of percolation that most affects the size of the clusters and therefore the optical response for longer wavelengths. For this reason, the approximation with the Bruggeman model allows to obtain a trend more adherent to the experimental data in the LWIR band that is sensitive to the larger clusters created by the percolative effects. These considerations on the spectral detection band dependence of the thermal bandwidth, with the aforementioned exemplary results, and the following evaluations on the theoretical modeling of the effective medium used to represent the vanadium dioxide metamaterial phase can be very useful in the fields of thermal camouflage, smart coatings for aerospace applications and thermal emitters.

Conflict of interest

The authors declared that there is no conflict of interest.

Acknowledgements

This work has been performed in the framework of an active collaboration between *Sapienza University of Rome* and the *Defence R&D Canada Valcartier* (P. Laou), and granted by "*FISEDA*" and "*SCHERMA*" projects – Italian Ministry of Defence.

References

[1] L.C. Hernandez-Mainet, M.A. Aguilar, M.C. Tamargo, C. Falcony, Design and engineering of IZO/Ag/glass solar filters for low-emissivity window performance, Opt. Eng. 56(2017) 105103. https://doi.org/10.1117/1.OE.56.10.105103.

[2] Z. Liu, Q. Sun, Y. Song, J. Yang, X. Chen, H. Wang, Z. Jiang, High-emissivity composite-oxide fillers for high temperature stable aluminum-chromium phosphate coating, Surf. Coat. Technol. 349(2018) 885-893. https://doi.org/10.1016/j.surfcoat.2018.06.028.

[3] J.W. Liu, J.J. Wang, H.T. Gao, Infrared Emissivities and Microwave Absorption Properties of Perovskite $La_{1-x}Ca_xMnO_3$ ($0 \leq x \leq 0.5$), Mat. Sci. Forum 914(2018) 96-101. https://doi.org/10.4028/www.scientific.net/MSF.914.96.

[4] J. Wei, Z. Wang, W. Chen, D.H. Cobden, New aspects of the metal-insulator transition in single-domain vanadium dioxide nanobeams, Nat. Nanotechnol. 4(2009) 420–424. https://doi.org/10.1038/nnano.2009.141.

[5] J. Morikawa, H. Takasu, M. Zamengo, Y. Kato, Micro-scale thermal imaging of CO2 absorption in the thermochemical energy storage of Li metal oxides at high temperature, Proc. SPIE 10214, 1021408(2017). https://doi.org/10.1117/12.2263079.

[6] M.C. Larciprete, Y.S. Gloy, R. Li Voti, G. Cesarini, G. Leahu, M. Bertolotti, C. Sibilia, Temperature dependent emissivity of different stainless steel textiles in the infrared range, Int. J. Therm. Sci. 113(2017) 130-135. https://doi.org/10.1016/j.ijthermalsci.2016.12.001.

[7] M.C. Larciprete, S. Paoloni, R. Li Voti, Y.S. Gloy, C. Sibilia, Infrared radiation characterization of several stainless steel textiles in the 3.5-5.1 μm infrared range, Int. J. Therm. Sci. 132(2018) 168-173. https://doi.org/10.1016/j.ijthermalsci.2018.04.024.

[8] E. Sakr , P. Bermel, Thermophotovoltaics with spectral and angular selective doped-oxide thermal emitters, Opt. Express 25(2017) A880-A895. https://doi.org/10.1364/OE.25.00A880.

[9] Y. Gong, Z. Wang, K. Li, L. Uggalla, J. Huang, N. Copner, Y. Zhou, D. Qiao, J. Zhu, Highly efficient and broadband mid-infrared metamaterial thermal emitter for optical gas sensing, Opt. Lett. 42(2017) 4537-4540. https://doi.org/10.1364/OL.42.004537.

[10] X. Wang, Y. Cao, Y. Zhang, L. Yan, Y. Li, Fabrication of VO_2-based multilayer structure with variable emittance, Appl. Surf. Sci. 344(2015) 230-235. https://doi.org/10.1016/j.apsusc.2015.03.116.

[11] C.O.F. Ba, S. T. Bah, M. D'Auteuil, V. Fortin, P.V. Ashrit, R. Vallée, VO2 thin films based active and passive thermochromic devices for energy management applications, Curr. Appl. Phys. 14(2014) 1531-1537. https://doi.org/10.1016/j.cap.2014.09.005.

[12] M. Holynska, A. Tighe, C. Semprimoschnig, Coatings and Thin Films for Spacecraft Thermo-Optical and Related Functional Applications, Adv. Mater. Interfaces 1701644(2018). https://doi.org/10.1002/admi.201701644.

[13] R. Zhang, S. Hu, C. Lu, Z. Xu, Bandgap engineering of $Gd_{0.8}Ca_{0.2}BaCo_2O_{5+\delta}$ double perovskite for photocatalysis applications, Ceram. Int. 44(2018) 15483-15489. https://doi.org/10.1016/j.ceramint.2018.05. 206.

[14] C.G. Granqvist, P.C. Lansåker, N.R. Mlyuka, G.A. Niklasson, E. Avendaño, Progress in chromogenics: new results for electrochromic and thermochromic materials and devices, Sol. Energy Mater. Sol. Cells 93(2009) 2032-2039. https://doi.org/10.1016/j.solmat.2009.02.026.

[15] F. J. Morin, Oxides Which Show a Metal-to-Insulator transition at the Neel Temperature, Phys. Rev. Lett. 3(1959) 34–36. https://doi.org/10.1103/PhysRevLett.3.34.

[16] A. Zylbersztejn , N.F. Mott, Metal-insulator transition in vanadium dioxide, Phys. Rev. B 11(1975) 4383. https://doi.org/10.1103/PhysRevB.11.4383.

[17] P. Markov, K. Appavoo, R.F. Haglund, S.M. Weiss, Hybrid Si-VO_2-Au optical modulator based on near-field plasmonic coupling, Opt. Express 23(2015) 6878-6887. https://doi.org/10.1364/OE.23.006878.

[18] S. Cueff, D. Li, Y. Zhou, F.J. Wong, J.A. Kurvits, S. Ramanathan, R. Zia, Dynamic control of light emission faster than the lifetime limit using VO_2 phase-change, Nat. Commun. 6(2015) 8636. https://doi.org/10.1038/ncomms9636.

[19] A. Hendaoui, N. Émond, S. Dorval, M. Chaker, É. Haddad, Enhancement of the positive emittance-switching performance of thermochromic VO_2 films deposited on Al substrate for an efficient passive thermal control of spacecrafts, Curr. Appl. Phys. 13(2013) 875-879. https://doi.org/10.1016/j.cap.2012.12.028.

[20] A. Hendaoui, N. Émond, S. Dorval, M. Chaker, É. Haddad, VO_2-based smart coatings with improved emittance-switching properties for an energy-efficient near room-temperature thermal control of spacecrafts, Sol. Energy Mater. Sol. Cells 117(2013) 494-498. https://doi.org/10.1016/j.solmat.2018.05.042.

[21] H. Ji, D. Liu, H. Cheng, C. Zhang, L. Yang, Vanadium dioxide nanopowders with tunable emissivity for adaptive infrared camouflage in both thermal atmospheric windows, Sol. Energy Mater. Sol. Cells 175(2018) 96-101. https://doi.org/10.1016/j.solmat.2017.10.013.

[22] D. Liu, H. Ji, R. Peng, H. Cheng, C. Zhang, Infrared chameleon-like behavior from VO_2(M) thin films prepared by transformation of metastable VO_2(B) for adaptive camouflage in both thermal atmospheric windows, Sol. Energy Mater. Sol. Cells 185(2018) 210-217. https://doi.org/10.1016/j.solmat.2018.05.042.

[23] L. Xiao, H. Ma, J. Liu, W. Zhao, Y. Jia, Q. Zhao, K. Liu, Y. Wu, Y. Wei, S. Fan, K. Jiang, Fast Adaptive Thermal Camouflage Based on Flexible VO_2/Graphene/CNT Thin Films, Nano Letters 15(2015) 8365-8370. https://doi.org/10.1021/acs.nanolett.5b04090.

[24] R. Macaluso, M. Mosca, V. Costanza, A. D'Angelo, G. Lullo, F. Caruso, C. Calì, F. Di Franco, M. Santamaria, F. Di Quarto, Resistive switching behaviour in ZnO and VO_2 memristors grown by pulsed laser deposition, Electron. Lett. 50(2014) 262-263. https://doi.org/10.1049/el.2013.3175.

[25] O.A. Novodvorsky, L.S. Parshina, A.A. Lotin, V.A. Mikhalevsky, O.D. Khramova, A. Cherebylo, V.Ya. Panchenko, Vanadium- and Titanium Dioxide-Based Memristors Fabricated via Pulsed Laser Deposition, J. Surf. Investig. X-Ra 12(2018) 322–327. https://doi.org/10.1134/S1027451018020313.

[26] M.A. Kats, R. Blanchard, S. Zhang, P. Genevet, C. Ko, S. Ramanathan, F. Capasso, Vanadium Dioxide as a Natural Disordered Metamaterial: Perfect Thermal Emission and Large Broadband Negative Differential Thermal Emittance, Phys. Rev. X 3 041004(2013). https://doi.org/10.1103/PhysRevX.3.041004.

[27] C.L. Gomez-Heredia, J.A. Ramirez-Rincon, J. Ordonez-Miranda, O. Ares, J.J. Alvarado-Gil, C. Champeaux. F. Doumas-Bouchiat, Y. Ezzahri, K. Joulain, Thermal hysteresis measurement of the VO_2 emissivity and its application in thermal rectification, Sci. Rep. 8(2018) 8479. https://doi.org/10.1038/s41598-018-26687-9.

[28] X. Li, L. Yang, S. Zhang, X. Li, J. Chen, C. Huang, VO_2(M) with narrow hysteresis width from a new metastable phase of crystallized Vo2(M)·0.25H_2O, Mater. Lett. 211(2018) 308-311. https://doi.org/10.1016/j.matlet.2017.09.105.

[29] S. Dou, W. Zhang, Y. Wang, Y. Tian, Y. Wang, X. Zhang, L. Zhang, L. Wang, J. Zhao, Y. Li, A facile method for the preparation of W-doped VO_2 films with lowered phase transition temperature, narrowed hysteresis loops and excellent cycle stability, Mater. Chem. Phys. 215(2018) 91-98. https://doi.org/10.1016/j.matchemphys.2018.05.018.

[30] L. Changshi, Z. Jianxin, Quantity comprehension of optical hysteresis loop, Optik 164(2018) 642-646. https://doi.org/10.1016/j.ijleo.2018.03.069.

[31] X. Li, S. Zhang, L. Yang, X. Li, J. Chen, C. Huang, A convenient way to reduce the hysteresis width of VO_2(M) nanomaterials, New J. Chem. 41(2017) 15260. https://doi.org/10.1039/C7NJ02632C.

[32] S. Chandra, D. Franklin, J. Cozart, A. Safaei, D. Chanda, Adaptive Multispectral Infrared Camouflage (2018), ACS Photonics 5(2018) 4513-4519. https://doi.org/10.1021/acsphotonics.8b00972.

[33] G. Leahu, R. Li Voti, C. Sibilia, M. Bertolotti, Anomalous optical switching and thermal hysteresis during semiconductor-metal transition of VO_2 films on Si Substrate, Appl. Phys. Lett. 103(2013) 231114. https://doi.org/10.1063/1.4838395.

[34] M. Tazawa, P. Jin, S. Tanemura, Optical constants of $V_{1-x}W_xO_2$ films, Appl. Optics 37(1998) 1858. https://doi.org/10.1364/AO.37.001858.

[35] J.C. Maxwell Garnett, VII. Colours in metal glasses, in metallic films, and in metallic solutions.-II, Phil. Trans. R. Soc. Lond. A 205(1906) 237-288. https://doi.org/10.1098/rsta.1906.0007.

[36] D.A.G. Bruggeman, Berechnung verschiedener physikalischer Konstanten von heterogenen Substanzen. I. Dielektrizitätskonstanten und Leitfähigkeiten der Mischkörper aus isotropen Substanzen, Ann. Phys. (Leipzig) 24(1935) 636. https://doi.org/10.1002/andp.19354160705.

[37] G. Bosi, F.E. Girouard, V. Truong, Extension of Maxwell-Garnett theory for granular surfaces, J. Appl. Phys. 54(1983) 1176. https://doi.org/10.1063/1.329972.

[38] H.S. Choi, J.S. Ahn, J.H. Jung, T.W. Noh, Mid-infrared properties of a VO_2 film near the metal insulator transition, Phys. Rev. B(1996) 54-7. https://doi.org/10.1103/PhysRevB.54.4621.

[39] A.V. Goncharenko, E.F. Venger, Percolation threshold for Bruggeman composites, Phys. Rev. E 70 057102(2004). https://doi.org/10.1103/PhysRevE.70.057102.

[40] G. Cesarini, G. Leahu, R. Li Voti, C. Sibilia, Long-wave infrared emissivity characterization of vanadium dioxide-based multilayer structure on silicon substrate by temperature-dependent radiometric measurements, Infrared Phys. Techn. 93(2018) 112-115. https://doi.org/10.1016/j.infrared.2018.07.032.

[41] H. Xiao, Y. Li, B. Fang, X. Wang, Z. Liu, J. Zhang, Z. Li, Y. Huang, J. Pei, Voltage-induced switching dynamics based on an AZO/VO_2/AZO sandwiched structure, Infrared Phys. Techn. 86(2017) 212-217.

[42] R. Li Voti, Optimization of a perfect absorber multilayer structure by genetic algorithms, J. Eur. Opt. Soc.-Rapid Publ.(2018) 14:11. https://doi.org/10.1186/s41476-018-0079-7.

[43] R. Li Voti, M.C. Larciprete, G. Lehau, C. Sibilia, M. Bertolotti, Optimization of thermochromic VO_2 based structures with tunable thermal emissivity, J. Appl. Phys. 112(2012) 034305. https://doi.org/10.1063/1.4739489.